A comparative study of platinum nanodeposits on HOPG (0001), MnO(100) and MnOx/MnO(100) surfaces by STM and AFM after heat treatment in UHV, O2 , CO and H2

Tsybukh, R.

CHAPTER 3

Growth modes, sintering mechanisms and equilibrium shape of small particles

This chapter provides a description of the growth modes of vapor-deposited material on a substrate along with an overview of the two key sintering mechanisms of small metal particles (clusters). The chapter continues with the issue of morphology and stability of small particles as well as the concept of "magic number" clusters and a brief discussion of the equilibrium particle's shape. The presented topics are used for the interpretation of experimental results presented in the following chapters.

3.1. Growth modes

Condensation of a substance from the vapor phase on a surface can result in various structures of the deposits, ranging from two and three-dimensional clusters to a completely closed layer. The system can be characterized by the specific surface free energies and interface energy. In the situation where the dependence of the surface free energy on the size and the shape of deposited material as well as the strain energy can be ignored on the basis of the Young-Dupré equation, the approximate magnitude of $\Delta\gamma$ (Fig. 3.1) guides the growth of a material on a substrate.

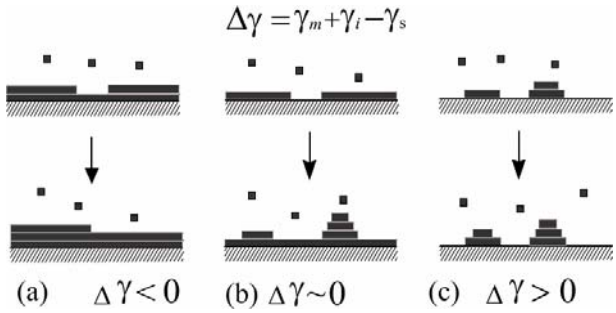

Figure 3.1: *Illustration of three growth modes of a material on a substrate: (a) Frank-van der Merwe; (b) Stranski-Krastanov; (c) Volmer-Weber.* γ_m *- the surface free energy of a material,* γ_s *- the surface free energy of a substrate,* γ_i *- the interface energy.*

Traditionally, the growth process of a deposited material can be subdivided into three modes [1]: a) the so-called *Frank-van der Merwe* mode, characterized

by a two-dimensional (2-D) growth. The substance grows on a surface by forming consecutive closed layers; b) the *Stranski-Krastanov* mode characterized by the formation of one or more monolayers (ML) followed by island growth; c) the *Volmer-Weber* (VW) growth with formation of three-dimensional structures. The surface may not be completely covered until a large deposition has been made. Layer plus island type of growth (b) is observed in some systems when the lattice parameter of the overlayer is slightly larger than the substrate. When several layers grow on each other at some point the strain inside the deposited layer may become too large to allow the growth of a homogenous layer. Small islands can emerge as a result of the interplay between strain and surface tension.

On the basis of only energy considerations the growth mode depends on the surface energies of substrate and adsorbate and on the interfacial energy. However, the principle of energy miniminization is not sufficient to predict the growth mode when the deposition does not occur under thermodynamic equilibrium conditions and kinetic considerations must be taken into account. On the basis of $\Delta\gamma$ alone it is quite difficult to predict the growth mode. One has to keep in mind that the electronic structure of a monolayer of a material is different than that of a bulk solid. As a result the surface free energy of a monolayer material can be different than the surface free energy of the bulk piece of this material.

3.2 Small particle growth and sintering mechanisms

In general, two mechanisms are responsible for the growth (sintering) of supported small particles: Ostwald ripening and Smoluchowski ripening. In the case of Ostwald ripening [2, 3], a difference of the two-dimensional gas atom density around clusters causes diffusion of adatoms around small clusters to the environment of large clusters. As a result the large clusters will grow at the expense of small clusters. In contrast, Smoluchowski ripening is caused by the migration of whole islands until they collide with other clusters, resulting in coalescence. This is assumed to be caused by diffusion of adatoms on the cluster surface, resulting in a displacement of the centre of mass. Small clusters are moving faster than large ones. After merging an energetically more stable cluster is formed.

3.2.1 Ostwald ripening

It is assumed that deposited particles form a spherical cap. The equilibrium concentration of adatoms c at a substrate close to a cluster depends on the radius

of curvature r and, therefore, on the size of the cluster. This is represented by the Gibbs-Thomson equation for an ideal two-dimensional gas [4]:

$$c(r) = c_{\infty} \exp\left(\frac{2\gamma\Omega}{k_B T r}\right) \tag{1}$$

where c_{∞} is the equilibrium concentration of an infinitely large cluster with a flat surface, γ is the surface free energy assumed to be isotropic, Ω is the atomic volume in the cluster and k_B and T are the Boltzmann constant and the temperature. From this equation it follows that the larger clusters are surrounded by a lower equilibrium adatom concentration than the smaller clusters. The flux of adatoms depends on the gradient in the adatom density and on an appropriate atomic mobility. Upon the assumption that attachment and detachment events of atoms to and from the clusters can be neglected, the diffusion process is the rate limiting factor for mass transport. The gradient in the adatom concentration at the interface with the clusters can be determined by the solution of the radial form of Fick's law. Here as boundary conditions the concentration at the interface with the clusters is given by eq. (1) and the concentration far away is equal to the average concentration c_{av}. This concentration is reached at a distance $l \times r$ from the cluster centre, where l is a dimensionless screening factor, which is assumed to be constant. Its introduction helps to overcome the difficulties with the divergence of the radial solution of Fick's law in two dimensions. The rate of cluster (of size r) growth from transport adatoms is given by the expression [4]:

$$\frac{\partial r}{\partial t} = \frac{\Omega D}{2\alpha_{\nu}(\theta) \ln l} \frac{1}{r^2} [c_{av} - c(r)], \tag{2}$$

where D is the diffusion constant of the adatoms on the substrate, $c(r)$ is the equilibrium concentration of the cluster as given by eq. (1) and $\alpha_{\nu}(\theta)$ is a geometrical factor that is used to account for the volume of a spherical cap [4].

The average concentration c_{av} is determined taking into consideration the mass-conservation in the system:

$$\int_0^{\infty} f(r,t) r^3 dr = \text{const.}, \tag{3}$$

where the probability distribution function of the cluster sizes $f(r,t)$ has to obey a continuity equation [4]:

$$\frac{\partial f(r,t)}{\partial t} = -\frac{\partial}{\partial r}\left(f(r,t)\frac{dr}{dt}\right), \tag{4}$$

where $\frac{dr}{dt}$ is given by eq. (2).

Retaining only the first term of the expansion of exponential function in eq. (1) and using eq. (2-4) upon assumption that for the majority of clusters the radius of curvature is large, one can obtain so-called universal power law expressions of an evolution of the average radius and cluster density. For instance, the growth of the average radius r as function of time t can be expressed as:

$$\bar{r}(t) = \bar{r}_0(1+kt)^{1/n} \tag{5}$$

where r_0 is the initial mean particle size at $t_0 = 0$.

Such relations lead to a so-called scaling behavior, which implies that the total number of clusters and the average size may change with time, but that the shape of the cluster size distribution does not change [4]. For Ostwald ripening n = 3 or n = 4 is expected. Thus, the value of n may directly point out to the growth mechanism. However, one has to keep in mind that n often can be temperature dependent. This phenomenon is not well understood yet.

3.2.2 Smoluchowski ripening

The mechanism of coalescence is determined by cluster diffusion. If atoms jump ν times per second over a distance a, the centre of mass of a cluster of s atoms jumps $n\nu$ times per second over a distance a, the centre of mass of a cluster of s atoms moves $n\nu$ times over a distance a/s. For the diffusion constant D of the adatoms over the surface we can write νa^2, resulting in a diffusion constant for the clusters $D_c = Dn/s^2$. For a hemispherical surface the movement of an atom has a component parallel to the substrate surface as well as perpendicular to the substrate surface. Therefore, a correction is required resulting in a diffusion constant for a hemispherical cluster:

$$D_c(r) = \frac{3\Omega^2\rho D}{\pi r^4} \tag{6}$$

In this formula ρ is the adatom density on the cluster surface and depends on the radius of curvature of the cluster. With ρ_∞ the adatom density on a flat surface is:

$$\rho(r) = \rho_\infty \exp\left(\frac{2\gamma\Omega}{k_B T r}\right) \tag{7}$$

Merging of clusters with a volume of s' and $s - s'$ results in an increase of the number of clusters with size s. Collisions between clusters of size s with any other cluster results in a decrease in their number. As a result one receives [5]:

$$\frac{\partial f(s,t)}{\partial t} = \int_0^r D_c(s') f(s',t) f(s-s',t) ds' - \int_0^\infty [D_c(s) + D_c(s')] f(s,t) f(s',t) ds' \qquad (8)$$

Using this equation it is possible to determine the evolution of the cluster size and density distributions.

Assuming that the adatom concentration ρ is independent of r and setting a particular shape of a cluster, one can deduce a range of power law expressions for the average cluster size and cluster density. These parameters, similar as in Ostwald ripening, obey scaling relations [5], but the shape of the size distribution in this case will be different. Hence, the size distribution may be a tool to distinguish between the two scenarios.

This issue was addressed by Jak *et al.* [6, 7] in the investigation of the cluster formation for the $Pd/TiO_2(110)$ system. They demonstrated that both mechanisms can be distinguished by the distribution of the cluster sizes and concluded that for this combination Smoluchowski ripening is the dominant process.

3.3 Morphology of small metal particles and "magic number" clusters

In general, atomic aggregates are classified into clusters (< 2 nm), consisting of two to several hundreds of atoms, and particles (with diameters 2-100 nm and more) [8]. The structure of clusters is determined by the number of atoms and their bonding, which can be of a different nature. Delocalized bonds of metal clusters are the reason of their close packed structures with maximum coordination number. The interaction energy between the atoms in metallic clusters is sufficiently well described by pairwise Lennard-Jones potential with r^{-6}, r - is the interatomic distance or, alternatively, by Morse potentials [9]. These two potentials consider only interaction between neighbor atoms. For more realistic modeling of metals, however, the pair potentials are not sufficient and many-body potentials are needed [10]. In very small clusters consisting of several atoms, due to different degree of orbitals hybridization, one can encounter an intermediate type of bonding. The consequence of this is that the physico-chemical properties of clusters are not a simple smooth function of their size. The stability of small clusters strongly depends on their size. Clusters with a specific number of atoms

"magic numbers" are extremely stable as reflected through the sequence of high and sharp peaks in the mass spectra of, for instance, homo-atomic metallic clusters [11]. "Magic clusters" possess high ionization potentials, low electron affinity, high symmetry and reduced reactivity, high melting points and large highest occupied molecular orbital–lowest unoccupied molecular orbital (HOMO-LUMO) gaps [12] as compared to clusters with one atom more or one atom less. "Magic number" clusters can be considered as superatoms, capable of forming compounds.

Over the last few decades the subject of "magic clusters" has been studied in detail, both theoretically and experimentally. Different kinds of clusters ranging from rare gases and metals to intermetallic and ionic compounds were screened. It is worth to mention recent impressive experimental results [13-16] concerning the observation of some small "magic number" clusters with STM. In general the determination of the "magic number" for different elements is not straightforward. In order to explain the observed "magic number" clusters and to describe their structure two approaches were developed.

The first approach takes into account the delocalized nature of valence electrons in metals [9]. The metal clusters are described as spherical droplets in which valence electrons behave similarly as free electron gas in bulk solid. The cluster's atomic nuclei with inner electrons are considered as positive cores forming uniform, structureless and for every valence electron equal background (jellium) [17-19]. These assumptions are justified for the clusters of the alkali and noble metals as their electronic structure is dominated by the number of valence electrons and the ionic cores are of secondary importance. The stability of a cluster in this model is determined not by its structure but by its electronic configuration. From this model it is impossible to predict the cluster structure. It gives relatively good predictions for the sp-bonded metals (alkali metals) clusters [20, 21].

The occurrence of certain cluster sizes in jellium model is explained by means of the quantum-mechanically defined electronic shell structure in which the electron shells degenerate and can be filled up by electrons according to the Pauli principle, every next electron must fill up the next higher energetic shell and is less bonded. Typical "magic clusters" with closed shells have 2, 8, 20, 40, 58, 92 … valence electrons [22].

The model describes a cluster with a central atom with closed shells as a close-packed structure. The radius of the metal droplet can be written as follows [23]: $R = r_{ws} \times N^{1/3}$ where N is the number of atoms in the droplet and r_{ws} is the Wigner-Seitz radius* of the element under consideration. For instance, the radius

* *The so-called Wigner-Seitz radius is the radius of a sphere whose volume is equal to the volume per atom in the solid [24]. For a general cubic crystal with j atoms in each unit cell and lattice constant a (for Pt: a=0.392 nm), the following relations*

of platinum (fcc metal) clusters consisting of 10, 55, 100 and 1000 atoms calculated with the above given formula is ~ 0.33, 0.58, 0.71 and 1.53 nm, respectively. The size of the clusters calculated according to the above expression agrees rather well with the size of clusters observed experimentally, e.g., for cubo-octahedral 55 Pt atom cluster by using transmission electron microscopy [26].

For very large clusters the influence of the electronic shells gradually decreases and the better stability of cluster of certain sizes is explained on the basis of geometrical packing effects. According to the geometrical approach, the "magic clusters" are the result of close-packing of atoms around the central atom. While growing very small clusters rearrange themselves into a completely new structure when an atom is added. However, this process cannot proceed infinitely and at some point an energetically preferred symmetry becomes frozen. One observes a minimum in the potential energy of free clusters described by a Lennard-Jones potential when dimers, trimers, tetramers are arranged at equal distance to each other. Thus, trimers form an equilateral triangle and tetramers - a tetrahedron [27]. Furthermore, from a geometrical point of view, a tetrahedral cluster can be considered as an "elementary building block" unit of more complex geometric structures which can be encountered in clusters. Eventually this can lead to the formation of several possible close packed structures consisting of 13 atoms: cuboctahedron, icosahedron, and hcp structure as shown in Fig. 3.2.

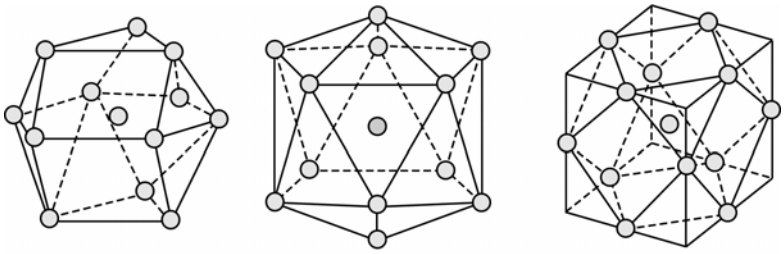

Figure 3.2: *Schematic illustration of different close packed structures consisting of 13 atoms: 1-hcp structure; 2-icosahedron; 3-cuboctahedron.*

Further growth takes place by adding layers of atoms to this 13-atomic core. Cuboctahedral and icosahedral clusters can grow by means of regular occupation the external surface of theses 13-atomic "seeds" with other the atoms. One layer is sometimes referred to as a geometric shell of atoms [28]. The shells

---

can be written: $a^3 = j \cdot \frac{4\pi}{3} \cdot r_{WS}^3 = V_{WS} \Leftrightarrow r_{WS} = \sqrt[3]{\frac{3}{4\pi \cdot j}} \cdot a$. *For a simple cubic (sc) structure j=1, for body-centered cubic (bcc) j=2 and for face-centered cubic (fcc) j= 4 [25].*

consist of equilateral triangles and in case of cuboctahedrons also from quadrates. For example, 13 is a "magic number" for rare gases, where clusters have icosahedral shape (optimum packing of spheres). This concept can be applied to the free clusters of, for example, noble gases as well as to supported clusters. As the latter ones are in contact with the support, this implies inevitably a deformation. The existence of "magic numbers" for atomic microclusters has been found experimentally for the first time in the mass spectra of free xenon clusters [29]. The clusters with 13, 55, and 147 atoms were observed that coincides with the numbers of spheres required for complete-shell icosahedra.

Each shell in a cubic (*ccp*) or hexagonal (*hcp*) close packed structure contains $10n^2 + 2$ atoms (n = number of the shell) [30]. Thus, for example, a cluster with n=1 has 13 atoms. The total number N of the elements (atoms) in a cluster that forms cuboctahedron or icosahedron can be calculated with the expression: $N_{(n)} = N_{(n-1)} + 10n^2 + 2$, $N_{(0)} = 1$ - central atom, n - number of a shell. Several of the first "magic number" clusters of cuboctahedral and icosahedral geometry are shown in Fig. 3.3.

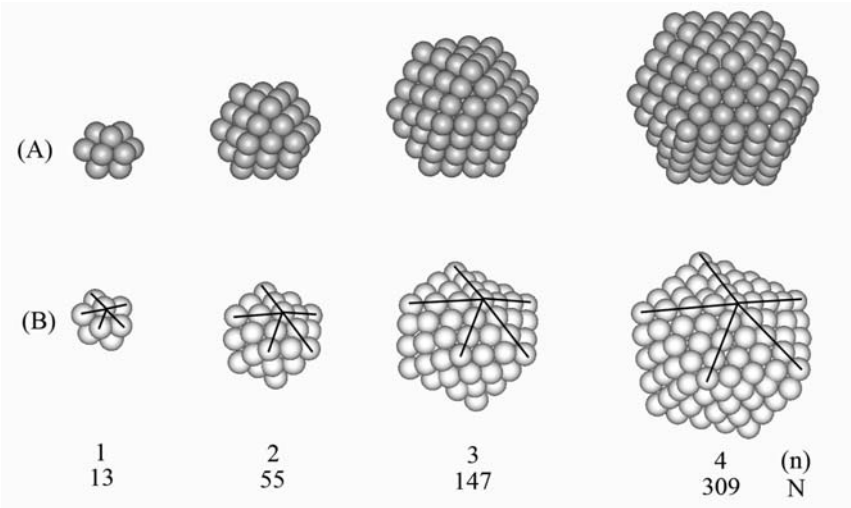

Figure 3.3: *Schematic representation of cuboctahedral (A) and icosahedral Mackay (B) "magic number" clusters.*

The cluster of 55 atoms within the second icosahedral shell occurs frequently and has been called Mackay icosahedron, or simply MI, which occurs not only in various homo-atomic clusters, but also in intermetallic compounds and quasicrystals [31].

"Magic clusters" quite often exhibit physical properties that are not characteristic to bulk material. For example, according to recent experiments [32],

Pt clusters as small as 13 atoms supported in the pores of a zeolite are magnetic in contrast to Pt atoms in the bulk platinum which are not magnetic.

The appearance of exceptionally stable "magic number" clusters of certain elements is explained by the simultaneous closure of electronic and geometric shells. Recently, the formation of this kind of "magic cluster" - Al_{13} [33] was detected. It is claimed that it can act as a single entity in chemical reactions, having properties similar to those of a halogen.

Besides homo-atomic "magic clusters" it is possible to produce hetero-atomic clusters as well. For example, Ziemann and Castleman [34] found that $(MnO)_x$ clusters for x = 3, 6, 9 and 12 exhibit prominent peaks in the mass spectra, indicating that these may be unusually stable.

It is important to note that the supported "magic clusters" not only deform as was mentioned above, but the specific interaction with the support may lead the formation of different "magic number" in two-dimensional systems, e.g., tetramers and hexagonal heptamers [35]. The formation of "magic clusters" which are stable at certain sizes on a particular surface is reviewed in [36]. Recently it was possible to register some of such "magic clusters" by STM [37, 38]. Nevertheless it must be noted that the exact geometrical structure of clusters is still difficult to access experimentally as well as theoretically [8, 39, 40]. For instance, less is known about the stability of clusters with sizes in between the "magic numbers". Theoretical calculations carried out using different potential models of the metal bond give different configuration of the lowest-energy isomer clusters [41-43]. For a very long-ranged potential the structures are not based on any regular packing [40]. The problem is also aggravated by the fact that the ground state energy of a cluster is situated on absolute or global minimum of the potential surface. Since the number of local minima in the potential energy surface increase exponentially with cluster size this makes localization of the true global minimum and thus the optimal cluster structure extremely difficult [44]. Recent advances in the description of matter aggregation and guiding principles of formation of the free and deposited atomic clusters including some of "magic number" are discussed in [11, 45]. The structure of clusters with less than 10 atoms cannot be fit to any model. For the transition metals, the structure must be determined on the basis of *ab initio* methods. Recent progress in the determination of the structure of unsupported small Pt_n (n=2-60) clusters using these methods can be found in [46-49].

In general, the actual morphology of clusters depends on many factors among which the most important are: the method of production, the growth kinetics, the time scale of the experiment. The structure of a cluster with lowest energy involves a balance between maximization of the number of nearest neighbors, whilst minimizing the strain energy that results from nearest neighbor

pair distances deviating from the equilibrium pair value. In the transition from small to larger sizes, at some given cluster size or certain geometric arrangements, clusters as described above can become unfavorable from an energetic point of view. If only nearest-neighbors are considered in the calculation of the surface energies, optimal atoms arrangement is given by the Wulff construction (see § 3.4), which describes the equilibrium shape of micro-crystallites. This approach can be used for small clusters with *fcc* structure [50]. For elements with *fcc* structure, the Wulff construction is a polyhedron: truncated octahedron with regular hexagonal faces.

As described in [51], the icosahedral structure is the equilibrium crystal shape (ECS) for small sizes and there is a critical size for the transition between icosahedron and *fcc* Wulff polyhedron. In addition, there are possible oscillations among *fcc* structures from Wulff polyhedron to octahedron and vice versa as a function of the cluster mass [50].

3.4 Equilibrium crystal shape. Wulff construction

The concept of ECS serves as a starting point to the understanding of the shape transformation of small crystallites and nanoparticles. It is also of fundamental importance to heterogeneous catalysis since certain chemical reactions are structure sensitive, i.e. proceed differently on different crystal surfaces [52-59].

The theory of ECS started with the work of Wulff [60] in which he showed that the normal distance from a common center of a small crystallite to any given surface facet is proportional to the surface free energy of that facet. In general, this statement can be expressed as follows:

$$\frac{\gamma_1}{h_1} = \frac{\gamma_2}{h_2} = \frac{\gamma_3}{h_3} \cdots \frac{\gamma_n}{h_n} = \frac{\gamma_i}{h_i} = const\ ,$$

where γ_i - is the specific surface free energy of the i^{th} crystal plane and h_i – is the central distance of the i^{th} crystal plane. Strictly, it is applicable only to the description of free-floating microscopic but not macroscopic crystallites at zero temperature, assuming that the crystallites are dislocation free and being in equilibrium that is rarely the case in real physical systems. Surface and volume stress in very small crystals ($<10^{-5}$ cm) can influence the ECS as well [61], implying that this approach is correct only for larger particles. This model also neglects some other physical effects, e.g., so-called 1/R effects.

In three dimensions, ECS can be defined in spherical coordinates by the distance r from the center of a sphere, and two polar angles φ and θ; then the surface free energy in terms of its orientation will be $\gamma(\varphi, \theta)$. However, for illustration, it is more convenient to represent ECS in two-dimensions. In this

case, the surface free energy, γ is a function of only one angle θ, $0 \le \theta \le 2\pi$, measured from some appropriate crystallographic direction. Thus, to construct the ECS at fixed temperature T, one needs [62] to start at the center of a crystallite W (Wulff point) and make the polar plot of the specific surface free energy $\gamma(\theta,T)$ as a function of local orientation θ relative to the crystal axes, to draw a radius vector in this direction, and then to construct the normal line to the radius vector at its intersection point with the polar plot and repeat the procedure at all orientations θ. The inner contour inside the polar plot will represent the ECS. Figure 3.4 (a) shows the 2-D cross section of the ECS (Wulff plot) for a crystalline body when only its nearest-neighbor interactions are considered [simple cubic lattice-gas model (see explanations further in the text)]. On the plot $\gamma(\theta)$ is anisotropic function and z(x) is the shape function. Cusped minima in certain

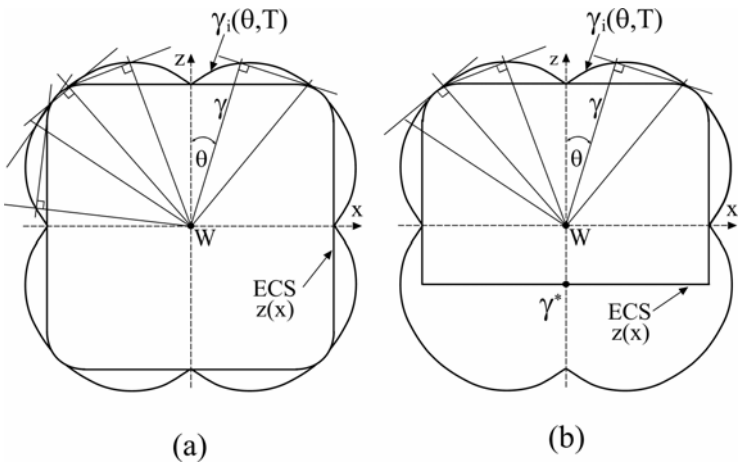

Figure 3.4: *Schematic illustration of the Wulff construction, connecting the anisotropic surface free energy γ(θ), outer curve, with the equilibrium crystal shape function z(x), inner curve. W - Wulff point. (a) Fourfold symmetric ECS of isolated crystallite. (b) Similar construction for a truncated crystallite supported by a substrate. Point γ* represents the interface and corresponds to the difference $\gamma_i - \gamma_s$. The figure is adopted from [63].*

directions correspond to surfaces of particularly simple structure. The analytic expressions for the transformation of anisotropic surface free energy γ - plot to ECS in two and three-dimensions can be found in [64]. In general, a Wulff plot can have missing orientations, sharp edges and corners, and its facets can be rounded or flat. The surfaces that possess the lowest surface free energy (commonly the dense atomic planes) shape the crystal in equilibrium. For instance, the ECS of a *fcc* crystal, at 0 K is a truncated octahedron (Wulff polyhedron) which only contains (111) and (100) faces. In reality the equilibrium shape of a crystallite is not necessarily reached and it can be determined

predominantly by kinetic or other nonequilibrium conditions. Since the surface free energy depends on temperature, an increase in temperature can result in a more round ECS. Hence, in addition to planar facets on ECS curved regions start to form, facets begin to diminish and at some temperature the ECS becomes everywhere smoothly round. Each type of facet vanishes at a characteristic roughening temperature. Analogous trends in ECS are observed when solid long-range interactions are introduced into the model. The more the range of the interaction energies is increased to more distant neighboring atoms, the more facets orientations are stabilized and high-index surfaces begin to appear. Examples of such calculations are shown in Table 3.1.

Table 3.1: *The surface energies at T=0 K for simple crystalline lattices with nearest neighbor interactions of energy J_1 and the second neighbor interactions of energy J_2. The energies are expressed in terms of the surface Miller indices {hkl}, the crystalline lattice constant a. The surfaces exposed on the ECS are listed in the final columns for the case of nearest neighbor interactions only, for the case of first and second neighbor interactions. A tabulation including third interactions, a large number of crystal habits can be found in [65].*

Structure $\gamma_{hkl}/[a^2\sqrt{h^2+k^2+l^2}]$		*Surfaces on ECS*	
		First neighbor interactions only	First and second neighbor interactions
Simple cubic	$\frac{1}{2}(h+k+l)J_1+(k+2l)J_2$	{001}	{001, {011}, {111}
Fcc	$2(h+2l)J_1+2(h+k+l)J_2$	{001}, {111}	{001, {011}, {111}
Bcc	$2lJ_1+(h+k+l)J_2$	{011}	{011}, {001}

The table is adopted from [63].

However, even regardless of the range of interaction at non-zero temperature commonly sharp edges and corners of ECS are rounded exposing a continuum of orientations. In dispersed supported catalysts small crystallites are supported on a substrate and it is important to know to what extend a substrate can influence their ECS. This question was resolved by Winterbottom [66] for faceted crystallites in contact with a flat solid surface. For a supported crystallite he defined the free energy of the surface in contact with the substrate as an effective surface energy: $\gamma^*(\theta)=\gamma_1(\theta)$ for the crystalline and $\gamma^*(\theta)=\gamma_i - \gamma_s,=-\gamma_1\cos(\theta_c)$ for the crystalline/substrate interface (the surface energy of the substrate and the surface energy of the interface are denoted γ_s and γ_i, respectively, and θ_c is the

contact angle at the interface). Due to the latter condition on the γ - plot appears an additional point and the function z(x) becomes truncated because of this interface condition. Figure 3.4 (b) depicts the construction of the ECS for a supported crystallite [$\gamma^*(\theta)$ is chosen to be positive]. Effective surface energy is a measure of the degree of wetting between the crystallite and the substrate. If $\gamma^*(\theta)$ is negative, Wulff's point W is located below the substrate surface and the γ^* point appears in the positive portion of the z-axis. If the contact angle is 180° or 0° one gets so-called non-wetting and complete wetting conditions, respectively, which represent nonphysical situations during the crystallite growth.

One should also keep in mind that the most probable crystallite shape is determined not only by the stability of planes, but also by the stability of atoms in the coordinatively most unsaturated sites (edges, corners). Frequently there is a situation where thermodynamically several types of planes are almost equally possible. Defect density either in the substrate or in the growing crystallite can also influence the crystal shape. The presence of defects can change the surface energy of a particular crystal plane. Depending on the amount of defects, differences in sizes of nanoparticles can result in a different balance between the surface energy of different crystallographic planes. Thus, a particle of a given size can have a different ratio of certain crystallographic planes than a particle of another size. The advent of scanning probe microscopy provided a valuable tool to investigate the ECS of crystallites of micron dimensions [67, 68].

3.5 References

[1] M. Zinke-Allmang, Thin Sol. Films **346,** 1-68 (1999).
[2] W. Oswald, Z. Phys. Chem. **34**, 495 (1900).
[3] R. D. Vingrenovitch, Acta Metall. **30**, 1079-1086 (1982).
[4] B. K. Chakraverty, J. Phys. Chem. Solids **28**, 2401-2412 (1967).
[5] D. Kandel, Phys. Rev. Lett. **79**, 4238-4241 (1997).
[6] M. J. J. Jak, C. Konstapel, A. van Kreuningen, J. Verhoeven, J. W. M. Frenken, Surf. Sci. **457** (3), 295-310 (2000).
[7] M. J. J. Jak, Ph. D. Thesis, Leiden University, The Netherlands (2000).
[8] Yu. I. Petrov, *Physics of Small Clusters*, (Nauka, Moscow, 1982) [in Russian].
[9] A. P. Sutton, *Electronic Structure of Materials*, (Clarendon Press, Oxford, 2004).
[10] C. L. Cleveland, U. Landman, J. Chem. Phys. **94** (11), 7376 (1991).
[11] L. C. Cune, M. Apostol, Digest Journal of Nanomaterials and Biostructures, **2**(4), 315-333 (2007).
[12] B. von Issendorff, O. Cheshnovsky, Ann. Rev. Phys. Chem. **56**, 549-580 (2005).

[13] V. G. Kotlyar, A. V. Zotov, A. A. Saranin, T. V. Kasyanova, M. A. Cherevik, O. V. Bekhtereva, M. Katayama, K. Oura and V. G. Lifshits, e-J. Surf. Sci. Nanotechnol. **1**, 33-40 (2003).
[14] S.-C. Li, J.-F. Jia, R.-F. Dou, Q.-K. Xue, Phys. Rev. Lett. **93**, 116103-1 [4 pages] (2004).
[15] H. H. Cheng, M. Y. Lai, J. H. Wei, C. M. Wei, Y. L. Wang, Nanotechnology, 2004. 4th IEEE Conference on, 498-501 (2004).
[16] M. A. K. Zilani, H. Xu, T. Liu, Y. Y. Sun, Y. P. Feng, X.-S. Wang, and A. T. S. Wee, Phys. Rev. B **73** (19), 195415 [5 pages] (2006).
[17] W. Ekardt, Z. Penzar, Phys. Rev. B **38**, 4273-4276 (1988).
[18] W. Ekardt, Phys. Rev. Lett. **52**, 1925-1928 (1984).
[19] M. Brack, Rev. Mod. Phys. **65**, 677-732 (1993).
[20] U. Röthlisberger, W. Andreoni, P. Giannozzi, J. Chem. Phys. **96** (2), 1248-1256 (1992).
[21] W. D. Knight, K. Clemenger, W. A. de Heer, W. A. Saunders, M. Y. Chou, M. L. Cohen, Phys. Rev. Lett. **52**, 2141-2143 (1984).
[22] J. W. Lee, G. D. Stein, J. Phys. Chem. **91**, 2450 (1987).
[23] R. L. Johnston, Phil. Trans. R. Soc. Lond. A **356**, 211-230 (1998).
[24] J. S. Blakemore, *Solid State Physics,* (Cambridge University Press, Cambridge, 1985).
[25] Christian Göransson, Master's Thesis, Linköping University, Sweden (2004).
[26] L. R. Wallenberg, J.-O. Bovin, A. K. Petford-Long, D. J. Smith, Ultramicroscopy **20**, 71-76 (1986).
[27] T. Laarmann, A. Kanaev, K. von Haeften, H. Wabnitz, R. von Pietrowski, T. Möller, J. Chem. Phys. **116** (17), 7558-7563 (2002).
[28] T. P. Martin, Phys. Rep. **273** (4), 199-241 (1996).
[29] O. Echt, K. Sattler, E. Recknagel, Phys. Rev. Lett. **47** (16), 1121-1124 (1981).
[30] R. Van Hardeveld, F. Hartog, Suf. Sci. **15** (2), 189-230 (1969).
[31] K. H. Kuo, Structural Chemistry **13** (3-4), 221-230 (2002).
[32] X. Liu, M. Bauer, J. van Slageren, H. Bertagnolli, E. Roduner Phys. Rev. Lett. **97**, 253401 (2006).
[33] D. E. Bergeron, A. W. Castleman, Jr. T. Morisato, S. N. Khanna, Science **304**, 84-87 (2004).
[34] P. Ziemann, A. W. Jr. Castleman, Phys. Rev. B **46**, 13480-13486 (1992).
[36] S. K. Nayak, P. Jena, V. S. Stepanyuk, W. Hergert, K. Wildberger, Phys. Rev. B **56**, 6952-6957 (1997).
[36] Y. L. Wang, M. Y. Lai, J. Phys.: Condens. Matter **13,** R589-R618 (2001).
[37] S. Tsukamoto, N. Koguchi, J. Cryst. Growth **209**, 258-262 (2000).
[38] V. G. Kotlyar, A. V. Zotov, A. A. Saranin, T. V. Kasyanova, M. A. Cherevik, I. V. Pisarenko, V. G. Lifshits, Phys. Rev. B **66** (16), 165401 [4 pages] (2002).

[39] J. A. Northby, J. Chem. Phys. **87** (10), 6166 (1987).
[40] J. E. K. Doye, D. J. Wales, Chem. Phys. Lett. **247,** 339-347 (1995).
[41] J. P. K. Doye, D. J. Wales, R. S. Berry, J. Chem. Phys. **103**, 4234-4249 (1995).
[42] J. P. K. Doye, D. J. Wales, J. Chem. Phys. **105** (18), 8428-8445 (1996).
[43] J. P. K. Doye, D. J. Wales, New J. Chem. 733-744 (1998).
[44] Yu. N. Shunin, A. V. Gopeyenko, Computer Modelling and New Technologies **9** (1), 15-31, (2005).
[45] L. C. Cune, M. Apostol, J. Theor. Phys. **82,** 1-15 (2002).
[46] K. Bhattacharyya, Ch. Majumder, Chem. Phys. Lett. **446** (4-6) 374 (2007).
[47] A. Sachdev, R. I. Masel, J. B. Adams, J. Catal. **136** (2), 320-333 (1992).
[48] A. Sebetci, Z. B. Güvenç, Surf. Sci. **525** (1-3), 66-84 (2003).
[49] R. C. Longo, L. J. Gallego, Phys. Rev. B **74**, 193409 [4 pages] (2006).
[50] C. Mottet, Ph. D. Thesis, CRMC2/CNRS, Marseille (1997).
[51] F. Baletto, C. Mottet, R. Ferrando, Surf. Sci. **446** (1), 31-45 (2000).
[52] A. Sasahara, H. Tamura, K. Tanaka, Catal. Lett. **28** (2-4), 161-166 (1994).
[53] A. Satsuma, R. Akahori, M. Kato, S-I. Komai, Y. H. T. Hattori, Mol. Catal. A **155** (1), 81-88 (2000).
[54] M. Myoung-Ki, J. Cho, K. Cho, H. Kim, Electrochim. Acta **45** (25), 4211- 4217 (2000).
[55] V. P. Zhdanov, Phys. Rev. B **64**, 193406 [4 pages] (2001).
[56] R. Barnes, I. M. Abdelrehim, T. E. Madey, Top. Catal. **14**, 53-61 (2001).
[57] H. Wilmer, M. Kurtz, K. V. Klementiev, O. P. Tkachenko, W. Grünert, O. Hinrichsen, A. Birkner, S. Rabe, K. Merz, M. Driess, C. Wöll and M. Muhler, Phys. Chem. Chem. Phys. **5**, 4736-4742 (2003).
[58] Y. Cui, H. Xu, Q. Ge, Y. Wang, S. Hou, W. Li, J. Mol. Catal. A **249** (1-2), 53-59 (2006).
[59] N. Semagina, A. Renken, D. Laub, L. Kiwi-Minsker, J. Catal. **246,** 308-314 (2007).
[60] G. Wulff, Z. Kryst. **34**, 449-530 (1901).
[61] N. Cabrera, Surf. Sci. **2**, 320-345 (1964).
[62] C. Hering, Phys. Rev. **82** (1), 87-93 (1951).
[63] H.-C. Jeong E. D. Williams, Surf. Sci. Rep. **34,** 171-294 (1999).
[64] D. Peng, S. Osher, B. Merriman, H.-K. Zhao, Contemporary Mathematics **238**, 251-303 (1999).
[65] G. A. Wolff, J. G. Gualtieri, Am. Mineral. **47**, 562-584 (1962).
[66] W. L. Winterbottom, Acta Metall.**15**, 303-310 (1967).
[67] H. P. Bonzel, Progr. Surf. Sci. **67**, 45-58 (2001).
[68] H. P. Bonzel, Phys. Rep. **385,** 1-67 (2003).